Liver sinusoidal endothelial cells constitute a major route for hemoglobin clearance

Gabriela Zurawska[1*], Zuzanna Sas[2*], Aneta Jończy[1*], Raghunandan Mahadeva[1], Patryk Slusarczyk[1], Marta Chwałek[1], Daniel Seehofer,[3] Georg Damm,[3] Maria Kulecka[4], Izabela Rumieńczyk[4], Morgane Moulin[5], Kamil Jastrzębski[1], Michal Mikula[4], Anders Etzerodt[5], Remigiusz Serwa[6], Marta Miączyńska[1], Tomasz P. Rygiel[7,#,$] and Katarzyna Mleczko-Sanecka[1,#,$]

[1] International Institute of Molecular and Cell Biology in Warsaw, Warsaw, Poland

[2] Medical University of Warsaw, Warsaw, Poland

[3] Department of Hepatobiliary Surgery and Visceral Transplantation, Clinic for Visceral, Transplant, Thoracic and Vascular Surgery, Leipzig University Medical Center, Leipzig, Germany

[4] Maria Sklodowska-Curie National Research Institute of Oncology, Warsaw, Poland

[5] Department of Biomedicine, Aarhus University, Aarhus, Denmark

[6] ReMedy International Research Agenda Unit, IMol Polish Academy of Sciences, Warsaw, Poland

[7] Mossakowski Medical Research Institute, Polish Academy of Sciences, Warsaw, Poland

*# equal contribution

$ To whom correspondence may be addressed:

Katarzyna Mleczko-Sanecka, International Institute of Molecular and Cell Biology in Warsaw, 4 Ks. Trojdena Street, 02-109 Warsaw, Poland, E-mail: kmsanecka@iimcb.gov.pl

or

Tomasz P. Rygiel, Mossakowski Medical Research Institute, Polish Academy of Sciences, 5 Pawińskiego Street, 02-106 Warsaw, Poland, E-mail: trygiel@imdik.pan.pl

Abstract

Mild rupture of aged erythrocytes occurs physiologically in the spleen, leading to the release of hemoglobin (Hb), while pathological hemolysis characterizes several diseases. The detoxification of Hb has traditionally been attributed to the sequestration of Hb-haptoglobin complexes by macrophages. However, this process remains incompletely studied in animal models or primary cells, leaving the precise mechanisms of Hb clearance elusive. Using mice and primary liver cell cultures (murine and human), we uncovered that Hb uptake is chiefly performed by liver sinusoidal endothelial cells (LSECs) and involves macropinocytosis. Consistently, mouse LSECs displayed proteomic signatures indicative of active heme catabolism, ferritin iron storage, antioxidant defense, and macropinocytic capacity. LSECs also exhibited high iron content and the expression of hepcidin-regulated iron exporter ferroportin. Using erythrocyte/Hb transfusion assays in mice, we demonstrated that while splenic macrophages excel in phagocytosis of erythrocytes, LSECs primarily scavenge Hb and Kupffer cells clear erythrocyte membranes, the spleen-borne hemolysis products delivered to the liver via the portal circulation. High-dose Hb injections resulted in transient hepatic iron retention, early LSEC-specific induction of heme-catabolizing *Hmox1* and iron-sensing *Bmp6*, culminating in hepcidin-mediated temporary hypoferremia. Transcriptional induction of *Bmp6* in mice was phenocopied by erythrocyte lysis upon phenylhydrazine or iron citrate injection, although the latter elicited a distinct LSEC transcriptional signature compared to Hb. In conclusion, we identify LSECs as key Hb scavengers, a function that establishes the spleen-to-liver axis for iron recycling and contributes to heme detoxification during hemolysis, coupled with the induction of the BMP6-hepcidin axis to restore iron homeostasis.

57 ## Introduction

58 Internal iron recycling from senescent red blood cells (RBCs) satisfies most of the body's iron
59 needs (1, 2) and relies chiefly on phagocytic clearance of aged RBCs by the splenic red pulp
60 macrophages (RPMs) (3, 4). However, recent evidence suggests that some aged RBCs escape
61 erythrophagocytosis and lyse locally in the spleen, thus releasing hemoglobin (Hb) (5). Several
62 inherited and acquired disorders, including hereditary anemias, autoimmune hemolytic
63 diseases, or infections, are characterized by compromised erythrocyte stability and increased
64 risk of hemolysis (6, 7). Free Hb is captured by the acute-phase plasma protein haptoglobin (8).
65 The Hb-haptoglobin complexes are sequestered via CD163 (9), a receptor that is highly
66 expressed by both splenic RPMs and liver macrophages, Kupffer cells (KCs) (1, 5). However,
67 the role of these macrophage populations in Hb uptake has not been well characterized.
68 Interestingly, pharmacokinetic studies in non-rodent mammals have shown that the clearance
69 rate of the Hb-haptoglobin complex is significantly slower than that of free Hb (10), and that
70 Hb sequestration may occur independently of haptoglobin and/or CD163 (11, 12). These
71 observations are clinically relevant as enhanced erythrophagocytosis and prolonged erythrolytic
72 conditions lead to the partial loss of the CD163-expressing iron-recycling macrophages (3, 13)
73 and are characterized by depletion of the plasma haptoglobin pool (7, 14, 15). Collectively, this
74 evidence suggests that macrophages may be dispensable for Hb clearance. It is well established
75 that free Hb undergoes renal glomerular filtration (16, 17). However, it remains unclear whether
76 other specialized routes of extra-renal and macrophage-independent Hb clearance operate in
77 the body.

78 The liver receives approximately 25% of the cardiac output and is exposed to the blood from
79 the portal circulation, which drains the gastrointestinal tract and the spleen (18). The hepatic
80 capillary network, composed of venous sinusoids, is specialized in monitoring and filtering the
81 blood components. Liver sinusoidal endothelial cells (LSECs), along with KCs, confer the most

82 efficient dual scavenging system in the body (19). While KCs engulf large particles, LSECs
83 remove macromolecules and nanoparticles, a function that protects the body from waste by-
84 products and noxious blood factors (20, 21). The maintenance of appropriate iron homeostasis
85 adds to the growing spectrum of homeostatic functions of LSECs. Importantly, LSECs are the
86 sensors of body iron levels and the major producers of the inducible angiokine bone
87 morphogenetic protein 6 (BMP6), and the homeostatic BMP2 (22, 23). BMPs function as
88 upstream activators of hepcidin, a key iron-regulatory hormone produced by liver hepatocytes
89 (2). Hepcidin suppresses iron release into the bloodstream via the sole known iron exporter
90 ferroportin (FPN), thereby limiting iron availability under iron-rich conditions (24). However,
91 it remains unclear how different types of iron signals are sensed and detoxified in the liver
92 microenvironment, and whether the emerging scavenging functions of LSECs cross-talk with
93 their role in maintaining iron homeostasis. Here, we show that LSECs constitute a major route
94 for Hb clearance. They contribute to steady-state iron recycling from spleen-derived Hb that
95 enters the liver via the portal vein and participate in heme detoxification during hemolysis,
96 timely coupled with the induction of the iron-sensing BMP6-hepcidin axis.

97

98

99

100

101

102

103

104 **Methods**

105 **Mice and *in vivo* procedures**

106 Female BALB/c mice (8-10 weeks old) were obtained from the Experimental Medicine Centre
107 of the Medical University of Bialystok or the Mossakowski Medical Research Institute of the
108 Polish Academy of Sciences. Female C57BL/6-Tg(UBC-GFP)30Scha/J (UBI-GFP/BL6) mice
109 were kindly provided by Aneta Suwińska (Faculty of Biology, University of Warsaw, Poland).
110 Female and male (8-12 weeks old) WT C57BL/6J and *Cd163*$^{-/-}$ mice were kindly provided by
111 Anders Etzerodt (Department of Biomedicine, Aarhus University, Denmark). For the dietary
112 experiment, C57BL/6J females (4 weeks old) were obtained from the Experimental Medicine
113 Centre of the Medical University of Bialystok. Mice were fed with a standard iron diet of 200
114 mg/kg (control) or a low iron diet containing <6 mg/kg (iron deficient) for 5 weeks before
115 analysis. All mice were maintained at the SPF facility under standard conditions (20°C,
116 humidity 60%, 12-h light/dark cycle). All data reporting the uptake of Hb by LSECs were
117 performed using female mice or primary female LSECs. However, we expect the findings to be
118 relevant for both sexes.

119 Proteins or their conjugates were dissolved in PBS and administered intravenously (*i.v.*) at the
120 dose indicated in the figure legends. For macrophage depletion, mice received *i.v.* solution of
121 liposomes containing clodronic acid (LIPOSOMA, #C-SUV-005) (5 ml/kg) or control empty
122 liposomes for 24 h. A sterile aqueous iron citrate (FeCit, 150 µg/mouse) solution (Sigma-
123 Aldrich, #F3388) or sterile citric acid buffer (0.05 M, Sigma-Aldrich, #251275) were
124 normalized to pH 7.0 and administered *i.v.* for 5 h. Mini-hepcidin (PR73, 50 nmol/mouse) (kind
125 gift from Elizabeta Nemeth, UCLA, USA) was injected intraperitoneally (*i.p.*) for 4 h. To
126 induce hemolysis, a sterile solution of phenylhydrazine (PHZ) (Sigma-Aldrich, #P26252) in
127 PBS was administered *i.p.* at a dose of 0.125 mg/g of body weight for 6 h. PKH26-stained
128 (Sigma Aldrich, #PKH26GL-1KT) temperature-stressed UBI-GFP RBCs were resuspended to

129 50% hematocrit in HBSS (Capricorn, #HBSS-1A) and administered *i.v.* for 1.5 h. PKH26-
130 stained RBCs ghosts were mixed with fluorescently labeled Hb (10 µg/mouse) and administered
131 *i.v.* for 1.5 h.

132 **Isolation of human non-parenchymal liver cells (NPCs)**

133 Liver tissue samples were obtained from the Department of Hepatobiliary Surgery and Visceral
134 Transplantation at Leipzig University Medical Center. Specimens were collected from
135 macroscopically healthy tissue adjacent to resected segments in patients with primary or
136 secondary liver tumors or benign local liver diseases. During resections, both diseased and
137 surrounding unaffected liver tissue were removed; a portion of this unaffected tissue was used
138 for liver cell isolation. All patients provided informed consent for tissue use in research,
139 following Leipzig University Hospital ethical guidelines (approval numbers 322/17-ek and
140 057/23-ek). Detailed protocols for cell isolation and further examination are provided in
141 Supplementary Methods.

142 **Cell-based and biochemical assays**

143 Isolation of murine and human NPCs for primary cell cultures together with cell treatments and
144 immunofluorescence are described in the Supplementary Methods. Isolation of cells from the
145 spleen, heart, bone marrow, and aorta, flow cytometry, FACS-sorting, liver tissue
146 immunofluorescence, heme/iron measurements, preparation of conjugated mouse Hb, stressed
147 RBCs, and RBC ghosts, and real-time quantitative PCR (RT-qPCR) were performed as
148 previously reported (25), or/and described in detail in Supplementary Methods.

149 **Statistics**

150 Data are represented as mean ± SEM. The number of mice/samples per group or the number of
151 independent cell-based experiments are shown in the figures. Statistical analysis was conducted
152 using GraphPad Prism software (Version 9.4.1). When two groups were compared two-tailed

153 unpaired Welch's t-test was applied, whereas for more groups, the One-Way or Two-Way
154 Analysis of Variance (ANOVA) with post-hoc Tukey's test for multiple comparisons was
155 performed, as indicated in figure legends. For all experiments, $\alpha=0.05$. Statistically significant
156 changes between means were indicated as follows: ns, not significant for $p>0.05$, * for $p<0.05$,
157 ** for $p<0.01$, *** for $p<0.001$, and **** for $p<0.0001$.

158 **Ethical Approval**

159 All animal experiments were conducted following the guidelines of European Directive
160 2010/63/EU and the Federation for Laboratory Animal Science Associations. The procedures
161 were approved by the Local Ethics Committee in Warsaw (No. WAW2/150/2019,
162 WAW2/138/2019, WAW2/137/2020, WAW2/137/2021, WAW2/179/2021, and
163 WAW2/094/2021), or for the dietary experiment by the local ethical committee in Olsztyn No.
164 26/2018. For the use of human cells, this study adhered to the Declaration of Helsinki and
165 received approval from the Ethics Committee of the Faculty of Medicine at Leipzig University
166 (Biobank of Surgical Research, registration no. 322/17-ek, 2020/06/10, ratified on 2021/11/30;
167 Role of human LSEC in hemoglobin clearance, registration no. 057/23-ek, 2023/08/21).

168 **Data availability**

169 Transcriptome analysis of LSECs was conducted using the AmpliSeq method and proteomics
170 was performed by label-free quantification with mass spectrometry as described in the
171 Supplementary Methods. LSEC transcriptomic data for iron citrate injection were previously
172 deposited in the GEO repository under accession no. GSE235976, whereas data for Hb injection
173 are accessible under no. GSE240270 (with a token: uhkrgywyhledjmj to allow for review).
174 Proteomics data were deposited to the ProteomeXchange Consortium via the PRIDE partner
175 repository with the dataset identifier PXD051274 (username: reviewer_pxd051274@ebi.ac.uk;
176 password: 0QJOAbzS for review).

177

178 ## Results

179 ### LSECs engage macropinocytosis to sequester Hb

180 Studies using radiolabeled Hb showed that the clearance of injected hemoglobin is rapid (16)
181 and mainly mediated by the liver, kidney, and spleen (16, 17). To address the involvement of
182 macrophages in Hb uptake, we first performed experiments using clodronate liposomes, a well-
183 established strategy that depletes tissue macrophages, including hepatic KCs. Using a whole-
184 organ imaging system, we observed that regardless of the KCs' presence, the liver emerged as
185 the major organ sequestering fluorescently-labeled mouse Hb (Fig. 1A and S1A and B). Next,
186 using flow cytometry and confocal microscopy imaging of mouse liver sections, we identified
187 $CD146^{+}STAB2^{+}$ LSECs as the major hepatic cell type that takes up Hb, surpassing KCs,
188 hepatocytes, and monocytes (Fig. 1B and C, Fig. S1C; see Data Supplements for gating
189 strategies). We found that murine primary LSEC cultures recapitulated a high capacity of this
190 cell type in Hb uptake, as validated by confocal microscopy and flow cytometry (Fig. 1D and
191 Fig. S1D). We further confirmed that human freshly isolated primary LSECs, distinguished by
192 CD36 and CD32B markers, as previously reported (26, 27) and confirmed by human Liver Cell
193 Atlas (28)(Fig. S1E), outperformed other NPCs in human Hb uptake (Fig. 1E and F). Of note,
194 flow cytometric analysis revealed that cells with high CD36 and CD23B expression, albeit not
195 highly abundant, showed the highest capacity for Hb scavenging (Fig. 1E).

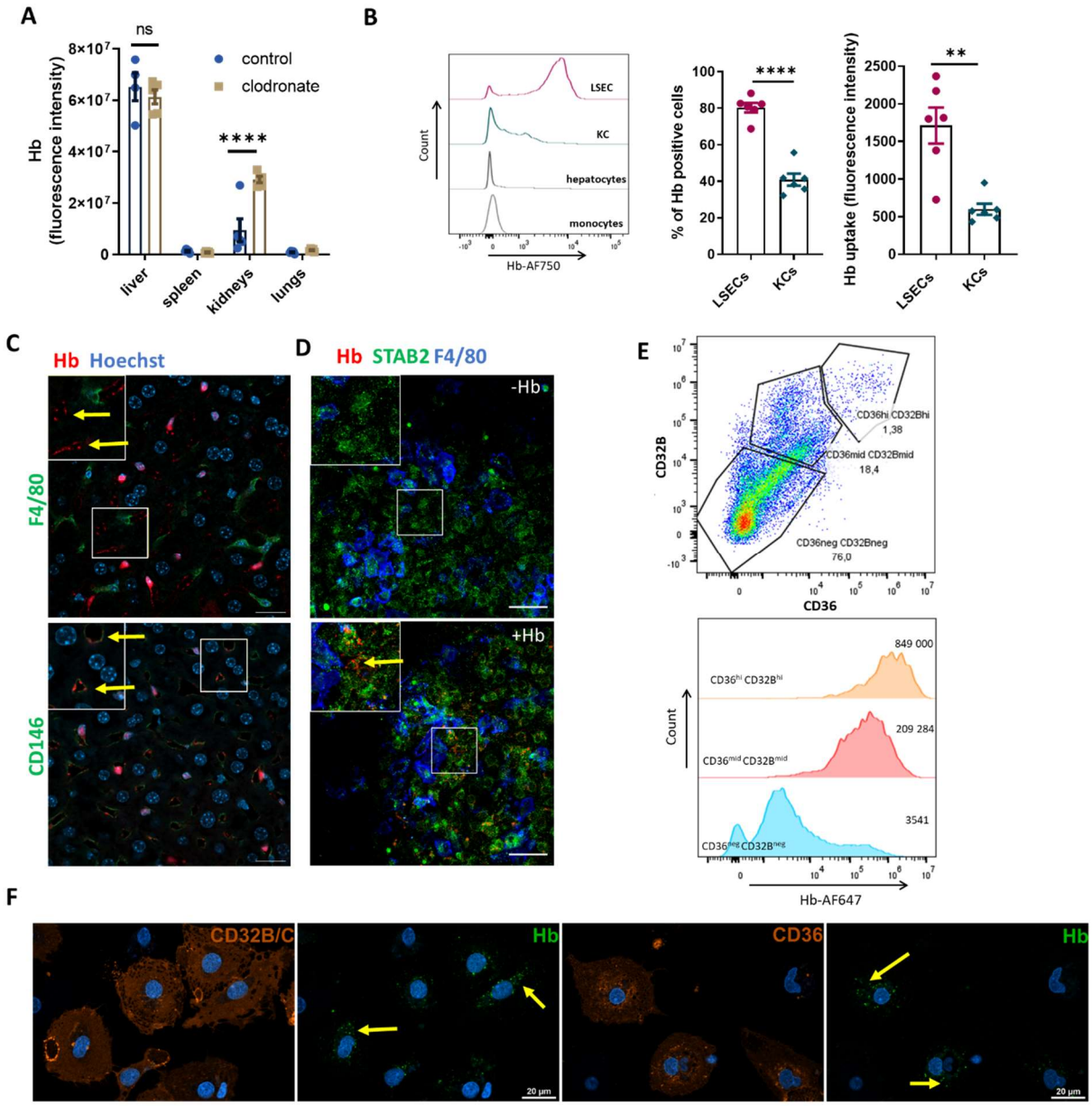

Figure 1. LSECs represent the major cell type that sequesters Hb.

(A) Hemoglobin (Hb) distribution in control and macrophage-depleted mice (clodronate) injected with Alexa Fluor 750-labeled Hb (Hb-AF750, 10 µg/mouse), imaged with Bruker *in vivo* Imaging System. Results are presented as total fluorescent counts from the isolated organs. (B) AF750 fluorescence from indicated liver cell populations isolated from Hb-AF750-injected mice was analyzed with flow cytometry. (C) Frozen liver slices from mice injected with Hb-AF647 (red) were processed and stained for Kupffer cells (KCs) (F4/80, green) or LSECs (CD146, green) and nuclei (blue). (D) Murine liver primary nonparenchymal cells (NPCs) were treated *in vitro* with Hb-AF750 (red) (0.5 µg/ml) and stained for F4/80 (blue) and the LSEC marker STAB2 (green). (C, D) Areas in the highlighted rectangles are shown at 5x higher magnification. (E) Flow cytometric analysis of human freshly isolated primary NPCs, exposed in culture to human Hb-AF647 and stained with the human LSEC markers CD36 and CD32B. The intensity of Hb-A647 uptake was measured in two LSEC subpopulations, more pure $CD36^{hi}CD32B^{hi}$ and $CD36^{mid}CD32B^{mid}$, as compared to other NPCs $CD36^{neg}CD32B^{neg}$. Numbers indicate MFI. Data are representative of three independent donors of human NPCs. (F) Hb-AF647

211 (green) uptake was imaged in freshly isolated human liver NPCs stained for the LSEC markers CD36
212 and CD32B (orange). (C, D, F) Arrows indicate Hb presence in LSECs; Scale bars, 20 μm. Numerical
213 data are expressed as mean ± SEM, each data point represents one biological replicate. Two-way
214 ANOVA with Tukey's Multiple Comparison tests was used in A, and Welch's unpaired t-test was used
215 to determine statistical significance in B; ns - not significant, **p<0.01 and ****p<0.0001.
216

217 To better understand the mechanism of Hb uptake we used mouse primary liver cell cultures.
218 In contrast to murine KCs, LSECs were negative for the Hb-haptoglobin complex receptor,
219 CD163 (Fig. 2A), and took up free Hb more robustly than the haptoglobin-bound Hb (Hb:Hp;
220 Fig. 2B). We, therefore, hypothesized that LSECs may sequester Hb in a receptor-independent
221 manner, possibly via macropinocytosis, a non-specific internalization of extracellular fluid (29).
222 Staining of primary murine LSECs with an early endosome marker, EEA1, identified many
223 constitutively formed intracellular vesicles of macropinosome size (1-2 μm) (Fig. 2C and S2A).
224 Fluorescently-labeled Hb was entrapped, though not exclusively, within such vesicles (Fig. 2C
225 and S2A), and co-localized with high-molecular-weight dextran, a known macropinocytic
226 cargo (Fig. 2D and S2B) (30, 31). Human primary CD36-high LSECs likewise displayed
227 numerous macropinosome-like vesicles and efficiently sequestered dextran (Fig. 2E and F).
228 Consistently, a well-established blocker of macropinocytosis, ethylisopropyl amiloride (EIPA),
229 in contrast to an inhibitor of clathrin-mediated endocytosis, chlorpromazine (CPZ), abolished
230 Hb uptake in murine primary LSECs (Fig. 2G and S2C) and decreased Hb scavenging by their
231 human counterparts (Fig. 2H). Likewise, Hb internalization by murine LSECs was partially
232 dependent on actin remodeling (suppressed by latrunculin A, LAT-A), and Cdc42 activity
233 (inhibited by ML141), both important for macropinosome formation (30). Hb uptake also
234 required canonical Wnt signaling via β-catenin (blocked by PRI-724), a pathway that is active
235 in LSECs (32) and has previously been shown to activate macropinocytosis (Fig. 2G) (33, 34).
236 Similarly, the uptake of Hb by human primary LSECs was suppressed by LAT-A (Fig. 2H).
237 Noteworthy, Hb uptake was not altered by the micropinocytosis blocker, nystatin (Fig. 2G).

238 Interestingly, close to 100% of LSECs actively sequestered even low Hb doses and the capacity
239 for the uptake did not show saturation with higher cargo presence, implying a receptor-
240 independent entry route (Fig. S2D). However, the same doses of dextran, a cargo of similar
241 molecular weight, were internalized by LSECs with far lower efficiency (Fig. S2D). This
242 implied a certain specialization of LSECs towards Hb scavenging, even though the uptake of
243 dextran by LSECs was likewise abolished by the macropinocytosis inhibitor EIPA or actin
244 remodeling blocker (Fig. S2E). Confirming the high macropinocytic capacity of LSECs *in vivo*,
245 we demonstrated their ability for efficient uptake of fluorescently-labeled albumin, another
246 known macropinocytic cargo (Fig. 2I) (31). Of note, we observed that the uptake of Hb by
247 primary murine KCs was not affected by the clathrin endocytosis inhibitor CPZ, and appeared
248 as dependent on macropinocytosis (Fig. S2F). Interestingly, the uptake of the Hb:Hp complex
249 by LSECs and KCs was suppressed by both EIPA and CPZ, implying the involvement of both
250 clathrin-endocytosis and macropinocytosis routes in this process (Fig. S2G). Taken together,
251 our data identify LSECs as efficient scavengers of both free and haptoglobin-bound Hb and
252 implicate macropinocytosis as an important alternative pathway for Hb uptake, which also
253 extends to KCs-mediated Hb scavenging.

254

255

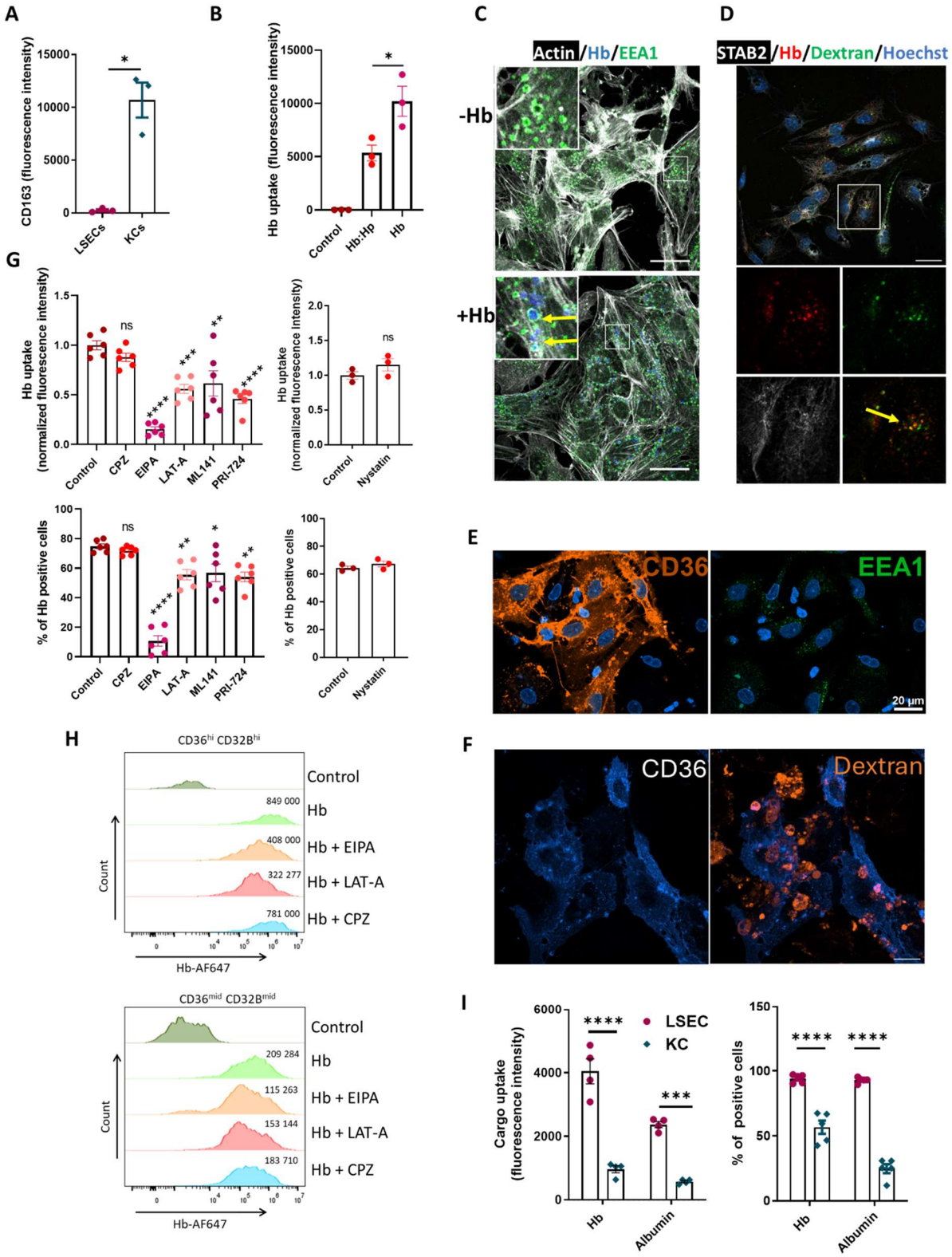

Figure 2. LSECs engage macropinocytosis to sequester Hb.

(A) Cell-surface expression of the CD163 receptor on LSECs and KCs was measured by flow cytometry and presented as fluorescence intensity. (B) Uptake of free Hb and Hb in the presence of haptoglobin (Hp, Hb:Hp) in primary murine LSEC cultures was measured with flow cytometry. (C) Hb-AF647 vesicle localization was imaged with microscopy in NPCs *in vitro* cultures depleted from macrophages. Arrows indicate Hb-AF647 (blue) presence in the EEA1^{+} (green) and Actin^{+} (white) vesicles. Areas in

263 the highlighted rectangles are shown at higher 5x magnification (left corner). Scale bars, 20 µm. (D) Co-
264 localization of Hb-AF647 (red) with rhodamine-dextran (green) was imaged with microscopy in
265 STAB2^{+} LSECs (white). Arrow indicates colocalization of Hb and rhodamine-dextran. The area in the
266 highlighted rectangle is shown at higher 5x magnification in separate channels below. Scale bar, 20 µm.
267 EEA1^{+} vesicles (E) and FITC-dextran uptake (blue) (F) were imaged with microscopy in human NPCs
268 cultures stained with the LSEC marker CD36. (G) NPCs were pre-treated with the clathrin-mediated
269 endocytosis inhibitor chlorpromazine (CPZ), the macropinocytosis blocker EIPA, actin polymerization
270 blocker latrunculin A (LAT-A), inhibitor of Cdc42 GTPase ML141, β-catenin inhibitor PRI-724 and
271 with micropinocytosis blocker nystatin before Hb-AF750 treatment for 10 min. Flow cytometry was
272 used to determine Hb uptake by the LSECs. (H) Flow cytometric analysis of CD36^{hi}CD32B^{hi} and
273 CD36^{mid}CD32B^{mid} human primary LSECs, treated with Hb-AF647 and exposed to EIPA, LAT-1 and
274 CPZ. Numbers indicate MFI. Data are representative of three independent donors of human NPCs. (I)
275 Mice were injected for 1 h with Hb-AF750 or albumin-AF750, both at 10 µg/mouse. The fluorescence
276 intensity of AF750, the percentage of AF750^{+} LSECs and KCs populations were measured with flow
277 cytometry. (C- F) Scale bars, 20 µm. Numerical data are expressed as mean ± SEM, each data point
278 represents one biological replicate. Welch's unpaired t-test was used to determine statistical significance
279 in A and G for nystatin, two-way ANOVA with Tukey's Multiple Comparison tests was used in I; while
280 one-way ANOVA with Tukey's Multiple Comparison tests was used in B and G. ns - not significant;
281 *$p<0.05$, **$p<0.01$, ***$p<0.001$ and ****$p<0.0001$.

282

283 **LSECs outperform other endothelial and macrophage populations in Hb uptake**

284 Similarly to the liver, sinusoidal endothelial cells are also present in the spleen and bone marrow
285 (20), organs that perform critical functions in systemic iron metabolism due to the presence of
286 CD163^{+} iron-recycling RPMs and erythroblastic island macrophages, respectively. Therefore,
287 we sought to accurately compare the Hb-scavenging capacity of endothelial and macrophage
288 populations from the spleen and bone marrow with that of hepatic LSECs and KCs over a wide
289 range of Hb doses. We used 1 µg of Hb, an amount below the binding capacity of circulating
290 haptoglobin (10-20 µg/ml plasma), an intermediate dose of 10 µg, and 100 µg (injected together
291 with 10 mg of unlabeled Hb), which saturates the haptoglobin pool and mimics hemolytic
292 conditions. We also injected mice with 1 µg of Hb bound to haptoglobin. Myeloid cells or ECs
293 of the bone marrow were not capable of efficient Hb sequestration (Fig. S3A). Strikingly, we
294 observed the extraordinary ability of LSECs to internalize Hb as compared to the other cell
295 types analyzed as exemplified by 70-99% of Hb-positive cells depending on the dose (Fig. 3A)

296 and the highest mean intensity of the Hb signal per cell as compared to KCs, splenic ECs, or
297 RPMs (Fig. 3B, D, F, H). The scavenging capacity of KCs and splenic ECs was gradually
298 increased with the Hb dose, (Fig. 3C-F), whereas RPMs contributed, albeit slightly, to the Hb
299 clearance only at the highest dose, mimicking hemolysis (Fig. 3G and H). Finally, using flow
300 cytometry and whole-organ imaging, we did not detect Hb accumulation in the aorta, lined by
301 non-sinusoidal ECs (Fig. S3B and C). In conclusion, our data suggest that LSECs outperform
302 other cell types in Hb clearance over a wide range of circulating Hb concentrations.

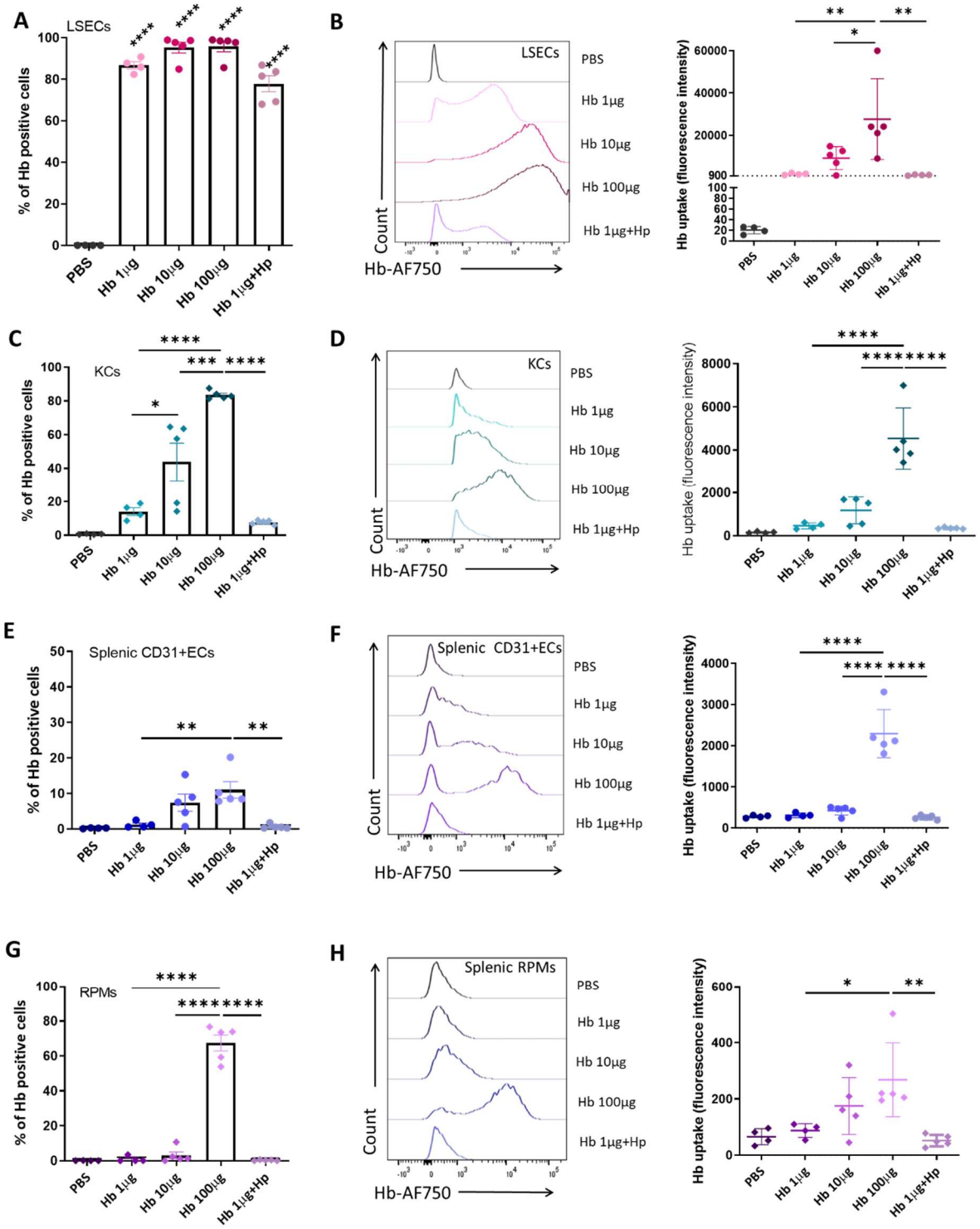

Figure 3. LSECs outperform other endothelial populations and macrophages in Hb uptake.

Percentage of Hb-AF750 uptake by mouse (A) LSECs, (C) KCs, (E) splenic endothelial cells (ECs), and (G) RPMs. Fluorescence intensity of Hb-AF750 in (B) LSECs, (D) KCs, (F) splenic ECs, and (H) RPMs. Both parameters were analyzed with flow cytometry. Data are expressed as mean ± SEM and each data point represents one biological replicate. One-way ANOVA with Tukey's Multiple Comparison tests was used to determine statistical significance; ns - not significant, *p<0.05, **p<0.01, ***p<0.001 and ****p<0.0001

311 **LSECs constitutively express proteins critical for iron recycling from heme**

312 We were intrigued by the fact that LSECs efficiently scavenge low doses of Hb. To further
313 explore their specialization, we examined data from single-cell RNA sequencing of ECs from
314 different mouse organs (35). Interestingly, both *Hmox1* [encoding heme oxygenase 1 (HO-1)]
315 and *Blrvb* (encoding biliverdin reductase b, BLRVB), genes important for heme catabolism,
316 together with important antioxidant enzymes such as *Gclc*, *Gpx4,* and *Nqo1*, were identified by
317 Kalucka et al. (35) as metabolic markers exclusively specific for liver EC. Using EC Atlas, we
318 visualized the expression levels of *Hmox1* and *Blvrb,* as well as of *Slc40a1*, the gene encoding
319 the iron exporter FPN, and found a clear signature for the high expression of these transcripts
320 in liver ECs compared to other organs (Fig. S4A). Consistently, by employing dedicated single-
321 cell RNA-seq databases we observed high expression levels of *Slc40a1*, *Hmox1* and *Hmox2* in
322 pig liver ECs and *Slc40a1* in human LSECs (Fig. S4B and C) (28, 36). Following up on these
323 transcriptomic signatures, we detected clear protein expression of FPN and HO-1 in the mouse
324 liver section (Fig. 4A) and primary murine LSECs (Fig. 4B). Further flow cytometric confirmed
325 a clear expression of cell-surface FPN on LSECs, reaching approx. 40% of cells, albeit
326 remaining at lower levels compared to KCs (Fig. 4C). Furthermore, close to 100% of LSECs
327 were positive for HO-1, although its expression levels appeared lower than in KCs (Fig. 4D).
328 Next, to obtain comprehensive information on LSEC adaptation to Hb clearance, we performed
329 label-free proteomic profiling of FACS-sorted LSECs in comparison to iron recycling
330 macrophages (RPMs and KCs) and splenic and heart ECs. This analysis identified 418 protein
331 groups significantly more abundant in LSECs than in splenic and cardiac ECs (Fig. 4E, Table
332 S1). Aside from well-established LSEC markers (STAB1, STAB2, CD206), intriguingly, these
333 included L and H ferritin, HO-1 and BLVRB, heme binding protein HEBP1, and enzymes
334 involved in antioxidant response (e.g., NQO1, GCLC or PRDX1). Interestingly, the hits
335 included also several known macropinocytosis effectors, such as Rabankirin-5, ATP6V0A1,

336 RAB5, or septin 2 (37-40), and several putative ones identified by previous RNAi screens (38)
337 (Table S1). This proteomic signature of LSEC, implying their active steady-state involvement
338 in Hb uptake and iron recycling from heme, was consistent with their relatively high labile iron
339 levels as compared to other ECs (Fig. 4F). FPN was robustly induced in LSECs under
340 conditions of systemic iron deficiency, mimicking the response observed in KCs (Fig. 4G),
341 suggesting a tight control of LSECs' FPN by circulating hepcidin. Confirming the iron-
342 exporting function of LSEC FPN, we detected a significant increase in labile iron in LSECs in
343 response to mini-hepcidin PR73 injection, a response even more pronounced than in KCs (Fig.
344 4H) (41). Collectively, these data indicate that LSECs are equipped with a protein machinery
345 that drives iron recycling from heme, suggesting their role in a steady-state iron turnover.

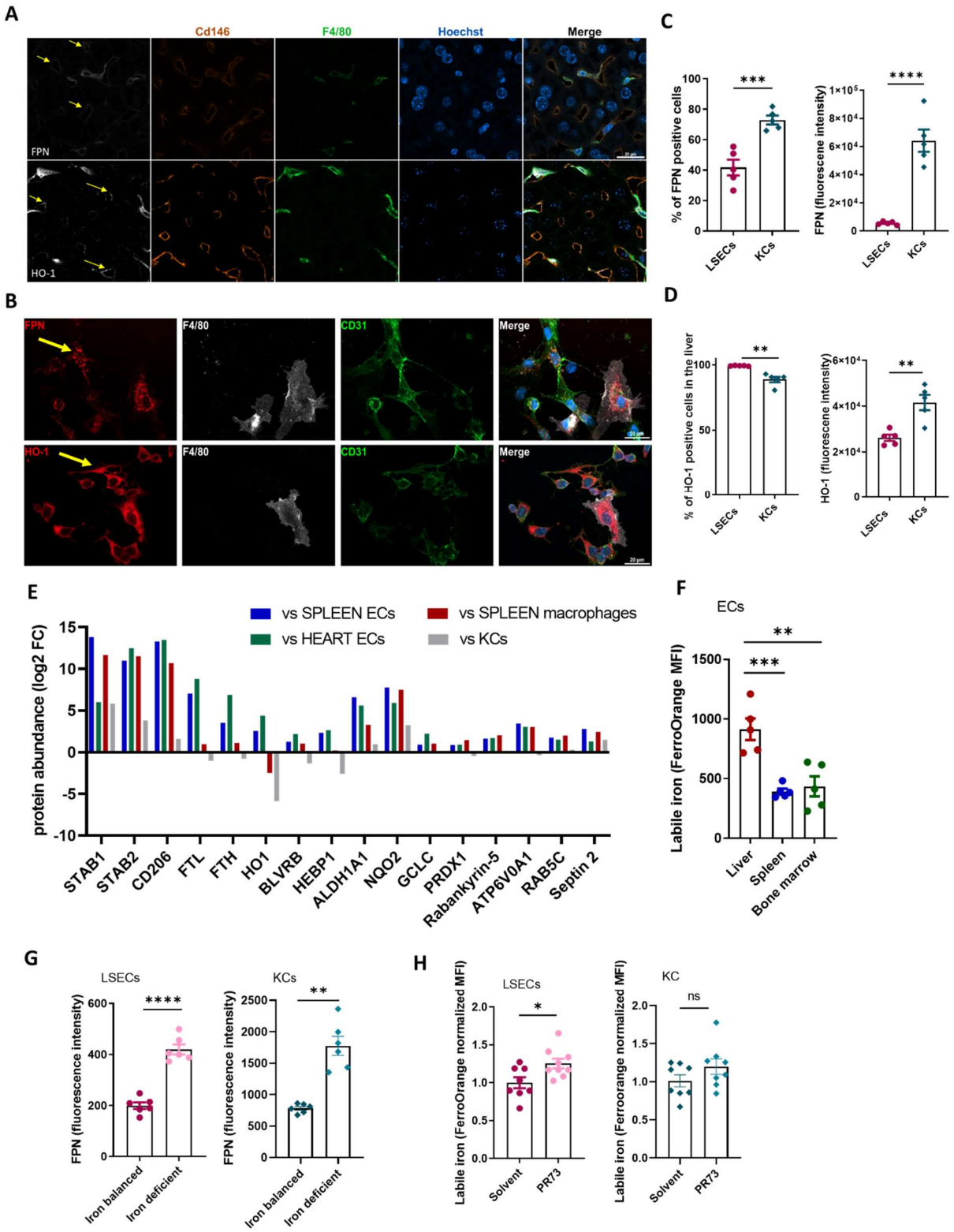

Figure 4. LSECs constitutively express proteins critical for iron recycling and macropinocytosis.

(A) Frozen mouse liver slices were processed and stained for FPN and HO-1 (white) in KCs (F4/80, green) or LSECs (CD146, orange). (B) FPN and HO-1 presence in F4/80^{+} (white) KCs and CD31+ endothelial cells (green) imaged by microscopy in murine NPC *in vitro* cultures. (A, B) Nuclei (blue), scale bars, 20 µm. Arrows indicate ECs positive for FPN or HO-1. (C) Flow cytometry analysis of FPN expression in LSECs and KCs. (D) Flow cytometry analysis of HO-1 expression in LSECs and KCs.

353 (E) Shown are selected proteins statistically significantly ($p<0.01$) more abundant in mouse FACS-
354 sorted LSECs than in spleen and heart endothelial cells (ECs). Log2 fold change (from 3 independent
355 cell isolates) in protein abundance in LSECs versus indicated cell type is presented. Individual label-
356 free quantification values of protein abundance and calculated p-values are included as Data
357 Supplements. (F) Cytosolic ferrous iron (Fe^{2+}) content in endothelial cells was measured with a
358 FerroOrange probe. (G) Flow cytometry analysis of FPN expression in LSEC and KCs isolated from
359 mice maintained on balanced or iron-deficient diets. (H) Cytosolic ferrous iron (Fe^{2+}) content was
360 measured with a FerroOrange probe in LSECs and KCs derived from mice injected with mini-hepcidin
361 (PR73). Numerical data are expressed as mean ±SEM and each data point represents one biological
362 replicate. Welch's unpaired t-test was used to determine statistical significance in C, D, G, and H; one-
363 way ANOVA with Tukey's Multiple Comparison tests was used in F; ns - not significant, *$p<0.05$,
364 **$p<0.01$, ***$p<0.001$ and ****$p<0.0001$.

365 **LSECs and KCs support iron recycling by removing hemolysis products from the spleen**

366 We next sought to understand how LSECs might be involved in physiological iron recycling.
367 The hemolysis-driven iron recycling model proposed by Klei et al. implied but did not formally
368 demonstrate that RPMs likely sequester spleen-derived Hb via highly expressed CD163 (5).
369 However, CD163 knock-out mice did not show major differences in systemic and splenic iron
370 parameters (Fig. S5). Inspired by the high capacity of LSECs for Hb scavenging, we
371 hypothesized that hepatic cells may play a role in the clearance of splenic hemolytic products
372 delivered via the portal circulation. We, therefore, extended previously reported studies by
373 quantifying the contributions of splenic and hepatic myeloid and endothelial cells to the uptake
374 of intact RBCs, RBCs devoid of cytoplasm (so-called RBC ghosts), and free Hb. To this end,
375 we injected mice with temperature-stressed RBCs, derived from Ubi-GFP transgenic mice and
376 stained with the membrane label PKH26 (Fig. 5A and B). This approach revealed that RPMs
377 outperformed other splenic cell types, F4/80^{high} CD11b^{high} pre-RPMs, CD11c^{+} dendritic cells
378 (DCs), monocytes, and splenic ECs in the sequestration of PKH26^{+}GFP^{+} intact RBCs. An equal
379 percentage of RPMs (approximately 30% of the population) were effective in removing
380 PKH26^{+}GFP^{-} RBC ghosts, a function that was efficiently supported by splenic pre-RPMs, and
381 to a lesser extent by DCs, monocytes, or ECs. Interestingly, we found that in the liver
382 phagocytosis of intact RBCs by KCs was less efficient than the uptake of RBC ghosts (Fig.

383 5B). No erythrophagocytosis of intact RBCs was detected in hepatic DCs and LSECs, but they
384 showed some capacity for the sequestration of RBC membranes, albeit lower than KCs.
385 Independently, injection of fluorescently-labeled RBC ghosts along with free Hb confirmed
386 that KCs and LSECs, respectively, rather than RPMs or splenic ECs, are specialized in the
387 clearance of these two major hemolysis products (Fig. 5C and D). Corroborating these data, we
388 detected an increase in heme levels in the portal vein plasma and we identified hemoglobin α
389 (HBA) and β (HBB) chains as top proteins upregulated in LSECs at the proteome-wide level
390 after injection of stressed RBCs compared to control PBS-injected mice (Fig. 5E and F).
391 Interestingly, among only 5 proteins that were significantly increased along with HBA and HBB
392 in LSECs following RBC transfusion, we detected two dehydrogenases ALDH1A1 and
393 ALDH1L1 (Fig. 5F), the former with established roles in the detoxification of aldehydes formed
394 by lipid peroxidation (42).

395 We next sought to determine whether the activity of LSECs to sequester Hb could be modulated
396 by the altered capacity of splenic RPMs to fully execute erythrophagocytosis. First, we
397 observed that LSECs became more effective at Hb uptake in response to macrophage depletion
398 after clodronate injection (Fig. 5G). Second, we took advantage of the physiological difference
399 in iron parameters between BALB/c and C57BL/6J (BL/6J) mice. We observed the lower
400 erythrophagocytic capacity of RPMs from BALB/c mice compared to BL/6J mice (Fig. 5H),
401 which was likely underlain by higher iron levels and reduced RPM FPN expression (Fig. S6A
402 and B), as reported previously (25). This led to heme accumulation in the extracellular space of
403 the spleen and portal plasma (Fig. 5I and S6C and D). This phenotype was coupled with
404 elevated levels of labile iron and higher FPN expression in LSECs of BALB/c mice (Fig. 5J
405 and K), indicating their enhanced activity in iron-recycling from Hb. Taken together, our
406 findings support a physiological role for LSECs in the sequestration of endogenous spleen-

derived Hb, thereby establishing a spleen-liver axis for effective iron recycling from senescent RBCs.

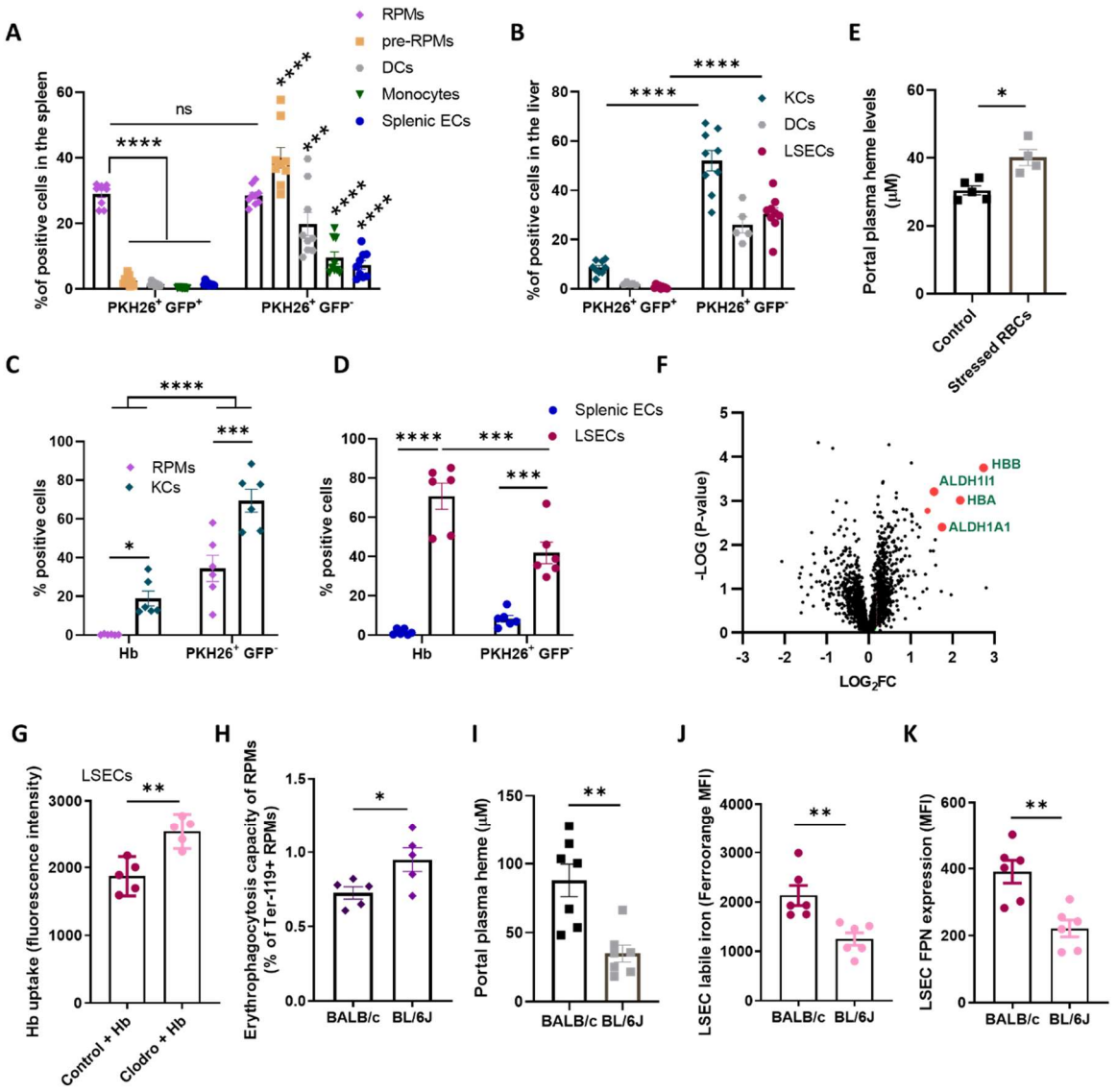

Figure 5. LSECs and KCs support iron recycling by removing hemolysis products from the spleen.

(A-D) Mice were administered i.v. with (A-B) stressed GFP$^+$ RBCs stained with a membrane marker PKH26 or (C-D) Hb-AF750 and PKH26$^+$ RBCs devoid of cytoplasm (RBC ghosts). Splenic and liver cells were isolated, stained, and analyzed by flow cytometry. (A) The percentage of cells positive for markers of intact RBCs (PKH26$^+$GFP$^+$) and RBC ghosts (PKH26$^+$GFP$^-$) in splenic RPMs, pre-RPMs, dendritic cells (DCs), monocytes, and endothelial cells (ECs). (B) The percentage of PKH26$^+$GFP$^+$ and PKH26$^+$GFP$^-$ cells in liver KCs, dendritic cells (DCs), and LSECs. (C-D) The percentage of cells positive for Hb (AF750) and RBC ghosts. (E) Heme levels from the portal vein plasma of control mice and mice transfused with temperature-stressed RBCs, measured by Heme Assay Kit. (F) Volcano plot illustrating the changes in the proteome of FACS-sorted LSECs 90 min after i.v. transfusion of stressed RBCs. Proteins significantly upregulated are marked in red. (G) Hb-AF750 uptake by LSECs derived from control and macrophage-depleted mice (Clodro). (H-K) BALB/c and C57BL/6J (BL/6J) mice

422 phenotype comparison. (H) The capacity of endogenous erythrophagocytosis was assessed by
423 intracellular staining of the erythrocytic marker (Ter-119) in RPMs. (I) Heme levels in the portal vein
424 were measured with Heme Assay Kit. (J) Cytosolic ferrous iron (Fe^{2+}) levels in LSECs were measured
425 with a FerroOrange probe. (K) FPN levels in LSECs measured by flow cytometry. Data are expressed
426 as mean ± SEM and each data point represents one biological replicate. Welch's unpaired t-test was
427 used to determine statistical significance in E, G-K; while two-way ANOVA with Tukey's Multiple
428 Comparison tests was used in A, B, C, and D; ns - not significant, *$p<0.05$, **$p<0.01$, ***$p<0.001$ and
429 ****$p<0.0001$.

430 **LSECs detoxify hemoglobin upon hemolysis and trigger the iron-sensing BMP6 angiokine**

431 We next set out to investigate the response of LSECs to hemolytic conditions. To this end, we
432 first injected mice with 10 mg of mouse Hb (equivalent to the RBC fraction in approximately
433 100 µl of blood) in a time-course manner. We detected a significant increase of heme iron
434 content in the liver at the early time point which was normalized by the 24-hour endpoint (Fig.
435 6A). Consistently, we observed a transient increase in iron levels in the liver, but not in the
436 spleen (Fig. 6B and S7A). Notably, the kidney also accumulated iron that could not be
437 mobilized and remained elevated throughout the experiment (Fig. S7B). Hemoglobin clearance
438 in the liver resulted in a strong transcriptional induction of the heme catabolizing enzyme
439 *Hmox1*, a response that could be attributed specifically to LSECs (Fig. 6C and D). The rapid
440 induction of *Hmox1* in LSECs upon intravenous Hb delivery was phenocopied by injecting the
441 mice with the hemolytic agent phenylhydrazine (PHZ) and exceeded by far the response of
442 KCs, splenic cells, and aorta (Fig. 6E and F). PHZ also caused a significant, albeit mild, iron
443 accumulation in the liver (Fig. 6G), but not in other organs (Fig. S7C and D).

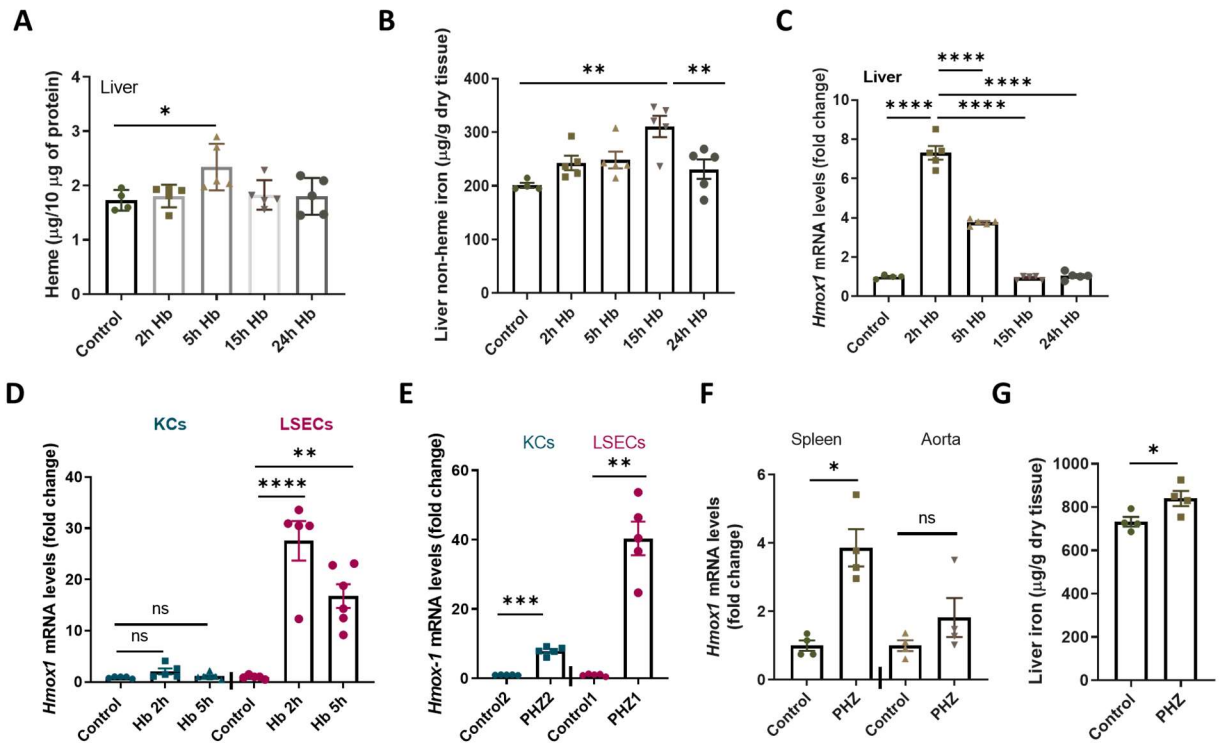

Figure 6. LSECs detoxify hemoglobin upon hemolysis.

(A-D) Mice were injected with native hemoglobin (Hb, 10 mg/mouse) and analyzed at indicated time points. (A) Heme iron levels in the liver were determined with Heme Assy Kit and normalized to protein content. (B) Non-heme iron content in the liver was measured by bathophenanthroline colorimetric assay. (C and D) *Hmox1* gene expression measurement by RT-PCR in (C) the liver and (D) FACS-sorted KC and LSEC populations. (E-G) Hemolysis was induced in mice by i.p. injection of phenylhydrazine (PHZ, 0.125 mg/g) 6 h before analysis. *Hmox1* gene expression in (E) FACS-sorted cell populations of KCs and LSECs, and (F) spleen and aorta. (G) Non-heme iron content in the liver. Data are expressed as mean ± SEM and each data point represents one biological replicate. One-way ANOVA with Tukey's Multiple Comparison tests was used in A-C, and separately for KCs and LSECs in D, while Welch's unpaired t-test was used to determine statistical significance in E-G, separately for each cell type/organ; ns - not significant, *p<0.05, **p<0.01, ***p<0.001 and ****p<0.0001.

Hemoglobin challenge rapidly increased the hepatic expression of the iron-sensing gene *Bmp6*, attributable to FACS-sorted LSECs, accompanied by the transient upregulation of the BMP target gene hepcidin (*Hamp*) in the liver (Fig. 7A-C). As expected, induction of the BMP6-hepcidin axis caused serum hypoferremia at the 15-h time-point which normalized after 24 h (Fig. 7D), reflecting the changes in liver iron content (Fig. 6B). Hemolysis induced by PHZ likewise led to the activation of *Bmp6* transcription in sorted LSECs (Fig. 7E). Finally, we aimed to determine whether LSECs induce a specific response when exposed to Hb compared to non-heme iron. To this end, we performed RNA sequencing to assess global gene expression

465 signatures upon injection of 10 mg of Hb and compared these to a previously reported response
466 to a quantitatively matched dose of iron citrate (43). Both stimuli induced *Bmp6* at very
467 comparable levels, and triggered an ETS1-controlled transcriptional program, as previously
468 reported for iron citrate response (43) (Fig. S8). Still, the two iron sources elicited different
469 responses of LSECs at the transcriptome-wide level (Fig. 7F). While only 64 genes, mainly
470 attributable to the response to oxidative stress and iron were co-induced by Hb and iron citrate,
471 as many as 372 and 202 genes increased their expression specifically upon Hb and iron citrate
472 injection, respectively (Fig. 7F). These differences were reflected by a largely distinct
473 functional enrichment within the Hb- and iron-induced transcriptional signature (Fig. 7G).
474 Interestingly, Hb-exposed LSECs specifically induced genes associated with immune and
475 inflammatory responses, such as the phagocyte marker *Cd68*, the chemokines *Ccl24*, *Ccl6,* and
476 *Ccl9*, and importantly, *Il18*, a cytokine implicated in the pathogenesis of the hemolytic sickle
477 cell disease (44). Furthermore, Hb ingestion activated gene expression signatures associated
478 with phagocytosis, the PI3K-Akt pathway, growth factor activity, and intracellular signaling,
479 enriched categories with several links to actin remodeling and, in some cases, directly to
480 macropinocytosis. Indeed, several genes induced by Hb, such as the receptors *Axl, Csf1r,* and
481 *Met*, the growth factors *Hgf* and *Pdgfa*, or the actin cytoskeleton-interacting factors *Evl* and
482 *Coro1a* are known to play a role in the regulation and/or execution of macropinocytosis (30,
483 45-47).
484 Collectively, these findings support the role of LSECs in Hb clearance and demonstrate their
485 high capacity to trigger the iron-sensing *Bmp6* angiokine in response to excessive Hb, along
486 with specific pro-inflammatory markers and factors associated with actin remodeling.

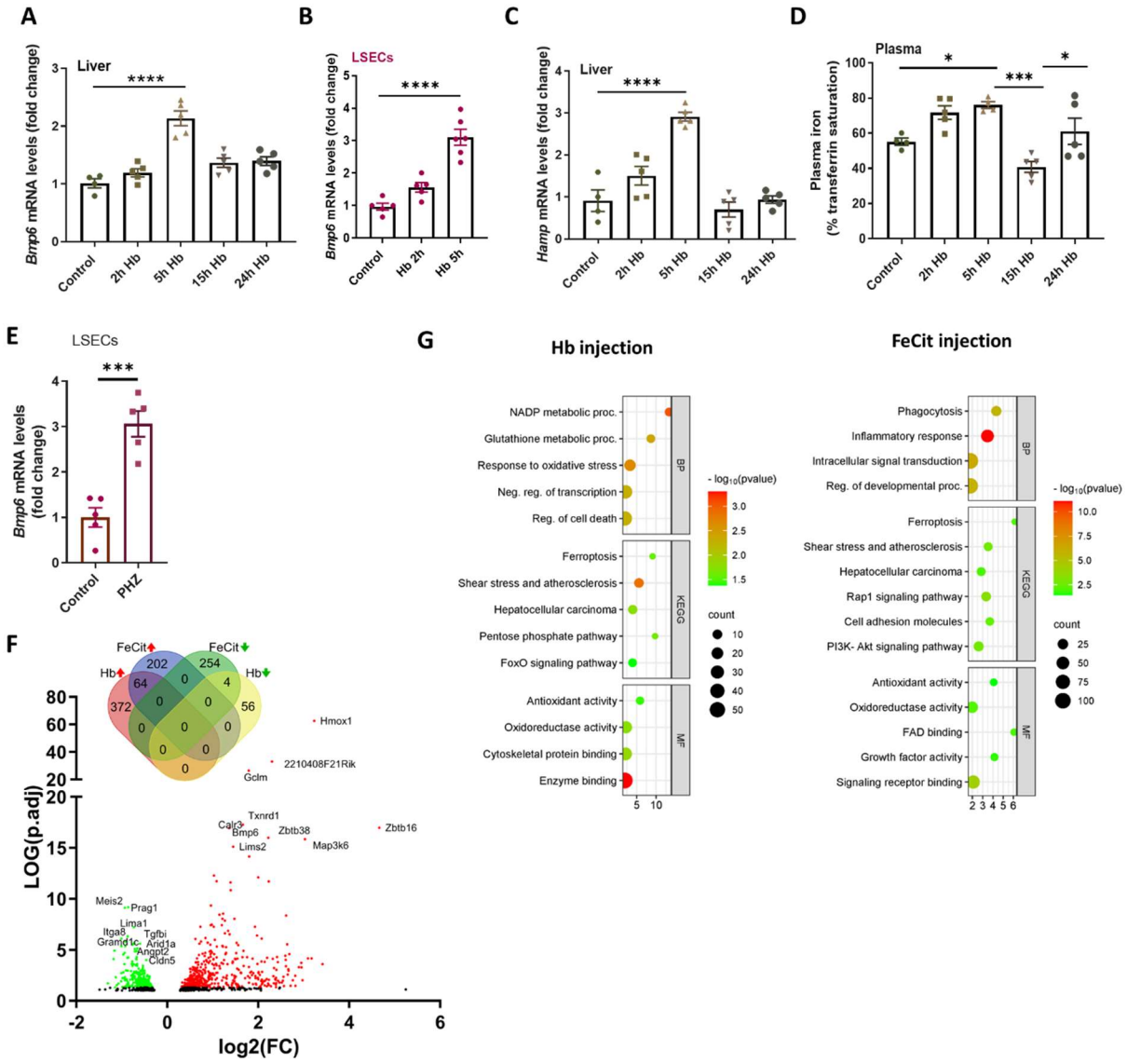

Figure 7. LSECs trigger the iron-sensing BMP6 angiokine upon hemolysis.

(A-D) Mice were injected with native hemoglobin (Hb, 10 mg/mouse) and analyzed at indicated time points. (A, B) *Bmp6* and (C) *Hamp* gene expression measured by RT-qPCR in whole livers or FACS-sorted LSECs, as indicated. (D) Plasma iron levels were determined by transferrin saturation measurements. (E) *Bmp6* expression in FACS-sorted LSECs in mice injected with (PHZ, 0.125 mg/g, 6 h). (F-G) Mice were injected with Hb (10 mg) or Ferric citrate (FeCit, 150 µg) for 5 h. (F) A volcano plot of differentially regulated genes identified by the RNA-seq transcriptomic analysis in FACS-sorted LSECs. The green color indicates negatively, and the red color positively-regulated genes. Venn diagram shows genes regulated by Hb and FeCit. (G) functional enrichment among genes induced by Hb or FeCit. The x-axis represents the fold of enrichment. The y-axis represents GO terms of biological processes (BP), Kyoto Encyclopedia of Genes and Genomes terms (KEGG), and GO terms of molecular function (MF). The size of the dot represents the number of genes under a specific term. The color of the dots represents the adjusted P-value. Data are expressed as mean ± SEM and each data point represents one biological replicate. One-way ANOVA with Tukey's Multiple Comparison tests was used in A-D, while Welch's unpaired t-test was used to determine statistical significance in E; ns - not significant, *p<0.05, ***p<0.001 and ****p<0.0001.

504 **Discussion**

505 Recent advances have revealed the critical role of the specialized hepatic sinusoidal
506 endothelium in maintaining systemic and liver homeostasis. The scavenging activity of LSECs
507 is essential for the hepatic clearance of biological macromolecules, such as denatured collagen,
508 glycans/glycation end products, modified low-density lipoproteins, small immune complexes,
509 lipopolysaccharides or viruses (20, 21, 27, 48, 49). In addition, LSECs regulate the vascular
510 tone in the liver, balance the tolerogenic immune milieu with the onset of immune responses,
511 ensure physiological zonation of hepatic immune cells (49, 50), and control iron balance by
512 producing the angiokines BMP2 and BMP6 (22, 23). Our study identifies the novel homeostatic
513 role of LSECs in the clearance of free Hb, an activity where their scavenging and iron-
514 regulatory functions converge.

515 The clearance functions of LSECs have been attributed to their extraordinary endocytic activity
516 and the surface expression of scavenger receptors (20). We discovered that LSECs have a
517 remarkable and constitutive capacity for macropinocytosis, similar to that of macrophages,
518 which use this pathway for antigen presentation, and in contrast to the inducible
519 macropinocytosis of cancer cells, which is critical for nutrient acquisition (29, 31). We show
520 that this capability distinguishes LSECs from ECs of other organs, thus significantly expanding
521 the scarce knowledge on the macropinocytic activity of ECs (51) and assigning physiological
522 significance to early observations that LSECs can engage macropinocytosis for antigen capture
523 (52). We propose that macropinocytosis of LSECs likely contributes to their scavenging
524 function. While this possibility merits future studies, macropinocytosis has recently been
525 identified as a major driver of LDL uptake by macrophages, leading to foam cell formation in
526 atherosclerosis (53). Hence, our findings aid in shifting the paradigm from the sole role of
527 scavenger receptor-mediated endocytosis in the clearance of blood-borne macromolecules,
528 emphasizing the importance of macropinocytic uptake. Further studies would be required to

529 address mechanistic details of how β-catenin signaling supports macropinocytosis of LSECs
530 and whether its pharmacological blockade would impair liver clearance functions. Finally, our
531 data also demonstrate that the macropinocytic activity of KCs supports their uptake of both free
532 Hb and Hb complexed with Hp, broadening the significance of this route in Hb clearance.

533 Our study employed *in vivo* approaches to verify the role of macrophages in Hb uptake and
534 revealed that LSECs qualitatively and quantitatively outcompete CD163-expressing KCs and
535 RPMs in this task. These provocative findings may be explained by the fact that the role of
536 CD163 in Hb uptake has been mainly investigated by its ectopic expression in non-macrophage
537 cells and by using polyclonal blocking anti-CD163 in cultured macrophages (9, 11, 54). Our
538 study does not exclude the contribution of iron-recycling macrophages to Hb uptake in
539 hemolytic conditions, nor does it imply that other tissues/endothelial cells are unaffected by
540 prolonged and pathological exposure to free Hb and heme (55). It remains to be determined to
541 what extent LSEC-mediated Hb uptake protects other organs in hemolytic disorders, such as
542 sickle cell disease or thalassemia, and whether and how LSEC functions are impaired in such
543 conditions. Noteworthy, CD163-expressing macrophages play important anti-inflammatory
544 roles, for example in the tumor microenvironment or arthritis, but these tissue-specific roles do
545 not appear to be related to Hb clearance (56-58). Finally, even though the clearance of free
546 circulating Hb was much faster than that of Hb-haptoglobin complexes in dogs (10), consistent
547 with our model, the CD163-independent uptake of Hb by LSECs in human cells would need to
548 be verified.

549 Most importantly, our study defines and quantifies the individual contribution of splenic and
550 hepatic cell types to physiological iron recycling. Consistent with previous studies (3, 4), we
551 provide evidence that RPMs are efficient at phagocytosis of intact stressed RBCs, whereas the
552 liver is the site of scavenging steady-state hemolytic products. KCs are efficient in the uptake
553 of RBC ghosts and outperform RPMs in the Hb uptake. LSECs, due to their anatomical location,

554 exceptional macropinocytic activity, and expression of the iron-recycling proteins, emerge as a
555 novel cell type involved in the maintenance of iron homeostasis, specialized for the removal of
556 spleen-derived Hb. Consistent with this newly proposed role of LSECs, it has been reported
557 that endothelial-specific FPN knock-out mice exhibit marked iron deficiency, develop anemia,
558 and show iron loading in liver NPC (59). Further studies using cell-type specific genetic
559 deletions of proteins involved in iron recycling would be crucial to quantify the exact
560 contribution of RPMs, KCs, and LSECs to the circulating plasma iron pool and thus assess their
561 relative involvement in iron recycling from RBCs.

562 **Authorship Contributions**

563 KMS, GZ, TPR, ZS, and MMia conceived and planned the experiments; ZS, GZ, AJ, PS, RM,
564 MC, IR, KJ, and MMo performed research; GZ, ZS, AJ, PS, RM, MC, MK, RS analyzed data;
565 GZ, ZS, AJ, PS, RM, MC, KJ, KMS, MMik, visualized data; AE provided CD163 KO mice,
566 DS and GD isolated and provided primary human NPCs; MMik and RS curated data; KMS,
567 TPR supervised the study; TPR, AJ, MMia and AE edited the manuscript; KMS, GZ, ZS wrote
568 the manuscript.

569 **Acknowledgments**

570 This work was funded by the National Science Centre grant 2018/31/B/NZ4/03676 to KMS
571 and the Foundation of Polish Science grant TEAM TECH/2016-1/8 to TPR. We express
572 gratitude to Marta Niklewicz for her substantial technical assistance in this project. We would
573 like to thank Daria Zdżalik-Bielecka for her valuable advice during the initial phases of the
574 project, and to Rafał Mazgaj for providing technical assistance in conducting experiments with
575 confocal microscopy. Additionally, we extend our thanks to Damian Strzemecki for his
576 technical assistance in performing mice injections. We thank Tara Arvedson (Amgen Inc. USA)
577 for the anti-ferroportin antibody, Elizabeta Nemeth for PR73, and Aneta Suwińska for sharing
578 UBI-GFP/BL6 mice. We thank Julian Connor Eckel for his excellent technical assistance in the

isolation and provision of primary human liver cells. Many thanks to Agnieszka Popielska and Anna Kosson, and the staff of the Experimental Medicine Centre (Bialystok, Poland) and Mossakowski Medical Research Institute (Warsaw, Poland) for their technical support. This research was performed thanks to the IIMCB IN-MOL-CELL Infrastructure (RRID: SCR_021630) funded by the European Union–NextGenerationEU under the National Recovery and Resilience Plan. IN-MOL-CELL Infrastructure was also funded by the European Union under Horizon Europe (Project 101059801 - RACE) and by the RACE-PRIME project carried out within the IRAP program of the Foundation for Polish Science co-financed by the European Union under the European Funds for Smart Economy 2021-2027 (FENG).

Conflict of Interest Disclosure

The authors declare that they have no conflict of interest.

References

1. Slusarczyk P, Mleczko-Sanecka K. The Multiple Facets of Iron Recycling. Genes (Basel) 2021;12.

2. Muckenthaler MU, Rivella S, Hentze MW, Galy B. A Red Carpet for Iron Metabolism. Cell 2017;168:344-361.

3. Youssef LA, Rebbaa A, Pampou S, Weisberg SP, Stockwell BR, Hod EA, Spitalnik SL. Increased erythrophagocytosis induces ferroptosis in red pulp macrophages in a mouse model of transfusion. Blood 2018;131:2581-2593.

4. Ma S, Dubin AE, Zhang Y, Mousavi SAR, Wang Y, Coombs AM, Loud M, et al. A role of PIEZO1 in iron metabolism in mice and humans. Cell 2021;184:969-982 e913.

5. Klei TRL, Dalimot J, Nota B, Veldthuis M, Mul FPJ, Rademakers T, Hoogenboezem M, et al. Hemolysis in the spleen drives erythrocyte turnover. Blood 2020;136:1579-1589.

6. Kato GJ, Steinberg MH, Gladwin MT. Intravascular hemolysis and the pathophysiology of sickle cell disease. J Clin Invest 2017;127:750-760.

604 7. Schaer DJ, Vinchi F, Ingoglia G, Tolosano E, Buehler PW. Haptoglobin, hemopexin,
605 and related defense pathways-basic science, clinical perspectives, and drug development. Front
606 Physiol 2014;5:415.

607 8. Wang Y, Kinzie E, Berger FG, Lim SK, Baumann H. Haptoglobin, an inflammation-
608 inducible plasma protein. Redox Rep 2001;6:379-385.

609 9. Kristiansen M, Graversen JH, Jacobsen C, Sonne O, Hoffman HJ, Law SK, Moestrup
610 SK. Identification of the haemoglobin scavenger receptor. Nature 2001;409:198-201.

611 10. Boretti FS, Baek JH, Palmer AF, Schaer DJ, Buehler PW. Modeling hemoglobin and
612 hemoglobin:haptoglobin complex clearance in a non-rodent species-pharmacokinetic and
613 therapeutic implications. Front Physiol 2014;5:385.

614 11. Schaer DJ, Schaer CA, Buehler PW, Boykins RA, Schoedon G, Alayash AI, Schaffner
615 A. CD163 is the macrophage scavenger receptor for native and chemically modified
616 hemoglobins in the absence of haptoglobin. Blood 2006;107:373-380.

617 12. Etzerodt A, Kjolby M, Nielsen MJ, Maniecki M, Svendsen P, Moestrup SK. Plasma
618 clearance of hemoglobin and haptoglobin in mice and effect of CD163 gene targeting
619 disruption. Antioxid Redox Signal 2013;18:2254-2263.

620 13. Theurl I, Hilgendorf I, Nairz M, Tymoszuk P, Haschka D, Asshoff M, He S, et al. On-
621 demand erythrocyte disposal and iron recycling requires transient macrophages in the liver. Nat
622 Med 2016;22:945-951.

623 14. Vinchi F, De Franceschi L, Ghigo A, Townes T, Cimino J, Silengo L, Hirsch E, et al.
624 Hemopexin therapy improves cardiovascular function by preventing heme-induced endothelial
625 toxicity in mouse models of hemolytic diseases. Circulation 2013;127:1317-1329.

626 15. Vinchi F, Sparla R, Passos ST, Sharma R, Vance SZ, Zreid HS, Juaidi H, et al. Vasculo-
627 toxic and pro-inflammatory action of unbound haemoglobin, haem and iron in transfusion-
628 dependent patients with haemolytic anaemias. Br J Haematol 2021;193:637-658.

629 16. Fagoonee S, Gburek J, Hirsch E, Marro S, Moestrup SK, Laurberg JM, Christensen EI,
630 et al. Plasma protein haptoglobin modulates renal iron loading. Am J Pathol 2005;166:973-983.

631 17. Marro S, Barisani D, Chiabrando D, Fagoonee S, Muckenthaler MU, Stolte J, Meneveri
632 R, et al. Lack of haptoglobin affects iron transport across duodenum by modulating ferroportin
633 expression. Gastroenterology 2007;133:1261-1271.

634 18. Poisson J, Lemoinne S, Boulanger C, Durand F, Moreau R, Valla D, Rautou PE. Liver
635 sinusoidal endothelial cells: Physiology and role in liver diseases. J Hepatol 2017;66:212-227.

636 19. Sorensen KK, McCourt P, Berg T, Crossley C, Le Couteur D, Wake K, Smedsrod B.
637 The scavenger endothelial cell: a new player in homeostasis and immunity. Am J Physiol Regul
638 Integr Comp Physiol 2012;303:R1217-1230.

639 20. Koch PS, Lee KH, Goerdt S, Augustin HG. Angiodiversity and organotypic functions
640 of sinusoidal endothelial cells. Angiogenesis 2021;24:289-310.

641 21. Schledzewski K, Geraud C, Arnold B, Wang S, Grone HJ, Kempf T, Wollert KC, et al.
642 Deficiency of liver sinusoidal scavenger receptors stabilin-1 and -2 in mice causes
643 glomerulofibrotic nephropathy via impaired hepatic clearance of noxious blood factors. J Clin
644 Invest 2011;121:703-714.

645 22. Koch PS, Olsavszky V, Ulbrich F, Sticht C, Demory A, Leibing T, Henzler T, et al.
646 Angiocrine Bmp2 signaling in murine liver controls normal iron homeostasis. Blood
647 2017;129:415-419.

648 23. Canali S, Zumbrennen-Bullough KB, Core AB, Wang CY, Nairz M, Bouley R, Swirski
649 FK, et al. Endothelial cells produce bone morphogenetic protein 6 required for iron homeostasis
650 in mice. Blood 2017;129:405-414.

651 24. Mleczko-Sanecka K, Silvestri L. Cell-type-specific insights into iron regulatory
652 processes. Am J Hematol 2021;96:110-127.

653 25. Slusarczyk P, Mandal PK, Zurawska G, Niklewicz M, Chouhan K, Mahadeva R, Jonczy
654 A, et al. Impaired iron recycling from erythrocytes is an early hallmark of aging. Elife 2023;12.

655 26. Strauss O, Phillips A, Ruggiero K, Bartlett A, Dunbar PR. Immunofluorescence
656 identifies distinct subsets of endothelial cells in the human liver. Sci Rep 2017;7:44356.

657 27. Ganesan LP, Kim J, Wu Y, Mohanty S, Phillips GS, Birmingham DJ, Robinson JM, et
658 al. FcgammaRIIb on liver sinusoidal endothelium clears small immune complexes. J Immunol
659 2012;189:4981-4988.

660 28. Guilliams M, Bonnardel J, Haest B, Vanderborght B, Wagner C, Remmerie A, Bujko
661 A, et al. Spatial proteogenomics reveals distinct and evolutionarily conserved hepatic
662 macrophage niches. Cell 2022;185:379-396 e338.

663 29. Canton J. Macropinocytosis: New Insights Into Its Underappreciated Role in Innate
664 Immune Cell Surveillance. Front Immunol 2018;9:2286.

665 30. Zdzalik-Bielecka D, Poswiata A, Kozik K, Jastrzebski K, Schink KO, Brewinska-
666 Olchowik M, Piwocka K, et al. The GAS6-AXL signaling pathway triggers actin remodeling
667 that drives membrane ruffling, macropinocytosis, and cancer-cell invasion. Proc Natl Acad Sci
668 U S A 2021;118.

669 31. Commisso C, Davidson SM, Soydaner-Azeloglu RG, Parker SJ, Kamphorst JJ, Hackett
670 S, Grabocka E, et al. Macropinocytosis of protein is an amino acid supply route in Ras-
671 transformed cells. Nature 2013;497:633-637.

672 32. Klein D, Demory A, Peyre F, Kroll J, Augustin HG, Helfrich W, Kzhyshkowska J, et
673 al. Wnt2 acts as a cell type-specific, autocrine growth factor in rat hepatic sinusoidal endothelial
674 cells cross-stimulating the VEGF pathway. Hepatology 2008;47:1018-1031.

675 33. Tejeda-Munoz N, Albrecht LV, Bui MH, De Robertis EM. Wnt canonical pathway
676 activates macropinocytosis and lysosomal degradation of extracellular proteins. Proc Natl Acad
677 Sci U S A 2019;116:10402-10411.

678 34. Redelman-Sidi G, Binyamin A, Gaeta I, Palm W, Thompson CB, Romesser PB, Lowe
679 SW, et al. The Canonical Wnt Pathway Drives Macropinocytosis in Cancer. Cancer Res
680 2018;78:4658-4670.

681 35. Kalucka J, de Rooij L, Goveia J, Rohlenova K, Dumas SJ, Meta E, Conchinha NV, et
682 al. Single-Cell Transcriptome Atlas of Murine Endothelial Cells. Cell 2020;180:764-779 e720.

683 36. Wang F, Ding P, Liang X, Ding X, Brandt CB, Sjostedt E, Zhu J, et al. Endothelial cell
684 heterogeneity and microglia regulons revealed by a pig cell landscape at single-cell level. Nat
685 Commun 2022;13:3620.

686 37. Dolat L, Spiliotis ET. Septins promote macropinosome maturation and traffic to the
687 lysosome by facilitating membrane fusion. J Cell Biol 2016;214:517-527.

688 38. Ramirez C, Hauser AD, Vucic EA, Bar-Sagi D. Plasma membrane V-ATPase controls
689 oncogenic RAS-induced macropinocytosis. Nature 2019;576:477-481.

690 39. Maxson ME, Sarantis H, Volchuk A, Brumell JH, Grinstein S. Rab5 regulates
691 macropinocytosis by recruiting the inositol 5-phosphatases OCRL and Inpp5b that hydrolyse
692 PtdIns(4,5)P2. J Cell Sci 2021;134.

693 40. Schnatwinkel C, Christoforidis S, Lindsay MR, Uttenweiler-Joseph S, Wilm M, Parton
694 RG, Zerial M. The Rab5 effector Rabankyrin-5 regulates and coordinates different endocytic
695 mechanisms. PLoS Biol 2004;2:E261.

696 41. Stefanova D, Raychev A, Deville J, Humphries R, Campeau S, Ruchala P, Nemeth E,
697 et al. Hepcidin Protects against Lethal Escherichia coli Sepsis in Mice Inoculated with Isolates
698 from Septic Patients. Infect Immun 2018;86.

699 42. Makia NL, Bojang P, Falkner KC, Conklin DJ, Prough RA. Murine hepatic aldehyde
700 dehydrogenase 1a1 is a major contributor to oxidation of aldehydes formed by lipid
701 peroxidation. Chem Biol Interact 2011;191:278-287.

702 43. Zurawska G, Jonczy A, Niklewicz M, Sas Z, Rumienczyk I, Kulecka M, Piwocka K, et
703 al. Iron-triggered signaling via ETS1 and the p38/JNK MAPK pathway regulates Bmp6
704 expression. Am J Hematol 2024;99:543-554.

705 44. Gupta A, Fei YD, Kim TY, Xie A, Batai K, Greener I, Tang H, et al. IL-18 mediates
706 sickle cell cardiomyopathy and ventricular arrhythmias. Blood 2021;137:1208-1218.

707 45. BoseDasgupta S, Moes S, Jenoe P, Pieters J. Cytokine-induced macropinocytosis in
708 macrophages is regulated by 14-3-3zeta through its interaction with serine-phosphorylated
709 coronin 1. FEBS J 2015;282:1167-1181.

710 46. Visweshwaran SP, Nayab H, Hoffmann L, Gil M, Liu F, Kuhne R, Maritzen T.
711 Ena/VASP proteins at the crossroads of actin nucleation pathways in dendritic cell migration.
712 Front Cell Dev Biol 2022;10:1008898.

713 47. Recouvreux MV, Commisso C. Macropinocytosis: A Metabolic Adaptation to Nutrient
714 Stress in Cancer. Front Endocrinol (Lausanne) 2017;8:261.

715 48. Malovic I, Sorensen KK, Elvevold KH, Nedredal GI, Paulsen S, Erofeev AV, Smedsrod
716 BH, et al. The mannose receptor on murine liver sinusoidal endothelial cells is the main
717 denatured collagen clearance receptor. Hepatology 2007;45:1454-1461.

718 49. Shetty S, Lalor PF, Adams DH. Liver sinusoidal endothelial cells - gatekeepers of
719 hepatic immunity. Nat Rev Gastroenterol Hepatol 2018;15:555-567.

720 50. Gola A, Dorrington MG, Speranza E, Sala C, Shih RM, Radtke AJ, Wong HS, et al.
721 Commensal-driven immune zonation of the liver promotes host defence. Nature 2021;589:131-
722 136.

723 51. Lin XP, Mintern JD, Gleeson PA. Macropinocytosis in Different Cell Types:
724 Similarities and Differences. Membranes (Basel) 2020;10.

725 52. Connolly MK, Bedrosian AS, Malhotra A, Henning JR, Ibrahim J, Vera V, Cieza-Rubio
726 NE, et al. In hepatic fibrosis, liver sinusoidal endothelial cells acquire enhanced
727 immunogenicity. J Immunol 2010;185:2200-2208.

728 53. Lin HP, Singla B, Ahn W, Ghoshal P, Blahove M, Cherian-Shaw M, Chen A, et al.
729 Receptor-independent fluid-phase macropinocytosis promotes arterial foam cell formation and
730 atherosclerosis. Sci Transl Med 2022;14:eadd2376.

731 54. Schaer CA, Schoedon G, Imhof A, Kurrer MO, Schaer DJ. Constitutive endocytosis of
732 CD163 mediates hemoglobin-heme uptake and determines the noninflammatory and protective
733 transcriptional response of macrophages to hemoglobin. Circ Res 2006;99:943-950.

734 55. Buehler PW, Humar R, Schaer DJ. Haptoglobin Therapeutics and
735 Compartmentalization of Cell-Free Hemoglobin Toxicity. Trends Mol Med 2020;26:683-697.

736 56. Etzerodt A, Tsalkitzi K, Maniecki M, Damsky W, Delfini M, Baudoin E, Moulin M, et
737 al. Specific targeting of CD163(+) TAMs mobilizes inflammatory monocytes and promotes T
738 cell-mediated tumor regression. J Exp Med 2019;216:2394-2411.

739 57. Etzerodt A, Moulin M, Doktor TK, Delfini M, Mossadegh-Keller N, Bajenoff M,
740 Sieweke MH, et al. Tissue-resident macrophages in omentum promote metastatic spread of
741 ovarian cancer. J Exp Med 2020;217.

742 58. Svendsen P, Etzerodt A, Deleuran BW, Moestrup SK. Mouse CD163 deficiency
743 strongly enhances experimental collagen-induced arthritis. Sci Rep 2020;10:12447.

744 59. Zhang Z, Guo X, Herrera C, Tao Y, Wu Q, Wu A, Wang H, et al. Bmp6 expression can
745 be regulated independently of liver iron in mice. PLoS One 2014;9:e84906.

746